MNRAS 000, 1–3 (2022) Preprint 23 May 2022 Compiled using MNRAS LATEX style file v3.0

Constraints on Dwarf Galaxy Evolution from Chemical Abundances

James W. Johnson,[1,2]★ Charlie Conroy,[3] Benjamin D. Johnson,[3] Phillip A. Cargile,[3] et al. (?)

[1] *Department of Astronomy, The Ohio State University, 140 W. 18th Ave., Columbus, OH, 43210, USA*
[2] *Center for Cosmology and Astroparticle Physics (CCAPP), The Ohio State University, 191 W. Woodruff Ave., Columbus, OH, 43210, USA*
[3] *Center for Astrophysics | Harvard & Smithsonian, 60 Garden Street, Cambridge, MA, 02138, USA*

Accepted XXX; Received YYY; in original form ZZZ

ABSTRACT

We develop a Bayesian method for fitting one-zone models of galactic chemical evolution to observed stellar abundances and ages. The two defining characteristics of this method are: (i) the likelihood of a given model-data pair of points is weighted by the star formation rate in the model, and (ii) for every data point, the likelihood is marginalized over the entire evolutionary history of the model. We demonstrate the accuracy of this method by means of mock data samples. These tests indicate that measurement precision and sample size are of similar importance in establishing the precision of the best-fit parameters, while stellar age information is of minimal importance. Indeed, even in the absence of age information, we find that this method produces accurate fits for (i) the timescales associated with the infall and star formation histories, and (ii) the total duration of star formation (i.e. quenching time) in a galaxy. We apply this new method to the Gaia-Sausage-Enceladus and the Sagitarrius dwarf Spheroidal, and we discuss how the best-fit parameters compare with existing measurements in the literature and the implications thereof.

Key words: methods: numerical – galaxies: abundances – galaxies: evolution – galaxies: star formation – galaxies: stellar content

1 METHODS

• We are interested in applying one-zone GCE models to dwarf galaxies and determining best-fit parameters. We begin by providing background on one-zone models, and then we select a parametrization from which we draw a fiducial mock stellar sample. We then use these data to introduce our fitting method.

1.1 One-Zone Models of Galactic Chemical Evolution

• The fundamental assumption of one-zone models is that newly produced metals mix instantaneously throughout the star forming gas reservoir. This approximation is valid as long as the mixing time-scale is negligible compared to the depletion time-scale (i.e. the average time an fluid element remains in the ISM before getting incorporated into new stars or ejected in an outflow). Based on the observations of Leroy et al. (2008), Weinberg, Andrews & Freudenburg (2017) calculate that characteristic depletion times can range from ∼500 Myr up to ∼10 Gyr for conditions in typical star forming disc galaxies. With the short length-scales and turbulent velocities of dwarf galaxies, instantaneous mixing should be a good approximation.

– If there's an observational reference of metal-mixing in the dwarf galaxy regime - specifically if the scatter in the [α/Fe]-[Fe/H] plane is dominated by observational uncertainty - Evan Kirby would probably be the one to know about it. If not, this would be a good thing to call out as a good observational test of the validity of the one-zone approximation.

• The assumption of instantaneous mixing eliminates the need for spacial information, reducing GCE to a system of coupled integro-differential equations which can be solved numerically.

1.1.1 *Inflows, Outflows, Star Formation, and Recycling*

• At a given moment in time, gas is added to the interstellar medium (ISM) via inflows and recycled stellar envelopes and is taken out of the ISM via outflows and new stars. This gives rise to the following differential equation describing the evolution of the gas-supply:

$$\dot{M}_{\rm g} = \dot{M}_{\rm in} - \dot{M}_{\star} - \dot{M}_{\rm out} + \dot{M}_{\rm r}, \tag{1}$$

where $\dot{M}_{\rm in}$ is the infall rate, $\dot{M}_{\star}$ is the star formation rate (SFR), $\dot{M}_{\rm out}$ is the outflow rate, and $\dot{M}_{\rm r}$ is the return of stellar envelopes from previous generations of stars.

– We relate the SFR to the gas supply by introducing the "star formation efficiency (SFE) timescale":

$$\tau_{\star} \equiv \frac{M_{\rm g}}{\dot{M}_{\star}}, \tag{2}$$

This quantity is often referred to as the "depletion time" in the observational literature (e.g. Tacconi et al. 2018). This nomenclature, taken from Weinberg et al. (2017), is based on its inverse $\tau_{\star}^{-1}$ often being referred to as the SFE itself because it describes the *fractional* rate at which some ISM fluid element is forming stars.

– There are various prescriptions for outflows in the literature. Some authors (e.g. Andrews et al. 2017; Weinberg et al. 2017)

★ Contact e-mail: johnson.7419@osu.edu

assume a linear proportionality between the two:

$$\dot{M}_{\rm out} \equiv \eta \dot{M}_{\star}. \tag{3}$$

Recently, de los Reyes et al. (2022) constrained the evolution of the Sculptor dwarf spheroidal galaxy with a linear proportionality between the SFR and the SN rate $\dot{N}_{\rm II} + \dot{N}_{\rm Ia}$. Kobayashi, Karakas & Lugaro (2020) developed a model in which outflow-driving winds develop in the early phases of the Milky Way's evolution, but die out on some timescale as the Galaxy grows. For modelling the Milky Way, some authors neglect outflows, arguing that they do not signicantly alter the chemical evolution of the disc (e.g. Spitoni et al. 2019, 2021). In our mock sample and in our fits to the GSE and the Sagitarrius dSph, we assume the linear proportionality given by equation (3). Our fitting routine, however, is easily extended to the parametrization of de los Reyes et al. (2022), and if outflows are to be neglected, one can simply take $\eta = 0$ in their fit.

– Weinberg et al. (2017) demonstrate that $\tau_\star$ and η determine the first-order details of the gas-phase evolutionary track in the [α/Fe]-[Fe/H] plane (see their Fig. 2). With low $\tau_\star$ (i.e. high SFE), nucleosynthesis is fast because star formation is fast, and a higher metallicity can be obtained before the onset of SN Ia than in lower SFE models. For this reason, $\tau_\star$ plays the dominant role in shaping the position of the knee in the [α/Fe]-[Fe/H] plane. As the galaxy evolves, it approaches a chemical equilibrium in which newly produced metals are balanced by the loss of metals to outflows and new stars. Controlling the strength of the sink term of outflows, η plays the dominant role in shaping the late-time equilibrium abundance of the model, which high outflow models (i.e. high η) predicting lower equilibrium abundances than their weak outflow counterparts. For observed data, the shape of the track itself directly constrains these parameters. The detailed form of the SFH has minimal impact on the shape of the tracks; rather, that information is encoded in the density of points along the evolutionary track and in the stellar metallicity distribution functions (MDFs).

– The recycling rate $\dot{M}_{\rm r}$, in general, depends on the stellar IMF (e.g. Salpeter 1955; Miller & Scalo 1979; Kroupa 2001; Chabrier 2003), the initial-final remnant mass relation (e.g. Kalirai et al. 2008), and mass-lifetime relation (e.g. Larson 1974; Maeder & Meynet 1989; Hurley, Pols & Tout 2000). A single stellar population returns some fraction of its initial mass r back to the ISM according to:

$$r(\tau) = \frac{\int_{m_{\rm to}(\tau)}^{u} (m - m_{\rm rem}) \frac{dN}{dm} dm}{\int_{l}^{u} m \frac{dN}{dm} dm} \tag{4}$$

where l and u are the lower and upper mass limits of star formation, respectively, $m_{\rm to}(\tau)$ is the turnoff mass of a stellar population of age τ, $m_{\rm rem}$ is the mass of a remnant left behind by a star of initial mass m, and dN/dm is the adopted IMF. Under this prescription, the recycling rate from *many* stellar populations, taking into account the full SFH, is given by:

$$\dot{M}_{\rm r} = \int_0^T \dot{M}_{\star} \dot{r}(T - t) dt \tag{5}$$

where T is the time in the model. Due to the steep nature of the mass-lifetime relation, the recycling rate is dominated by young stellar populations. Weinberg et al. (2017) demonstrate that it is sufficiently accurate in one-zone models to assume that some fraction $r_{\rm inst}$ of a stellar population's initial mass is returned to the ISM immediately (see their Fig. 7; they recommend $r_{\rm inst} = 0.4$ for a Kroupa 2001 IMF, and $r_{\rm inst} = 0.2$ for a Salpeter 1955 IMF). Although it is simpler to assume $\dot{M}_{\rm r} = r_{\rm inst} \dot{M}_{\star}$, numerical integration of equations (4) and (5) is easy, and `VICE` already does it, so we stick with that.

1.1.2 Core Collapse Supernovae

1.1.3 Type Ia Supernovae

1.1.4 Asymptotic Giant Branch Stars

1.1.5 Nucleosynthetic Yields

1.2 A Fiducial Mock Sample

- In this section, we define a fiducial mock sample by sampling individual stars from a one-zone model of known parameters and adding artificial uncertainty. We then use this fiducial sample to describe our fitting technique in § 1.3. We then discuss how the accuracy and precision of the recovered best-fit parameters is affected by sample size and measurement precision.
- We take an exponential infall history described by

$$\dot{M}_{\rm in} \propto e^{-t/\tau_{\rm in}} \tag{6}$$

with $\tau_{\rm in} = 2$ Gyr and an initial gas mass of 0. The overall normalization of the infall history is irrelevant because mass information cancels in one-zone models when you compute abundances. We additionally select $\tau_\star = 15$ Gyr and $\eta = 10$. We set the onset of star formation $\tau = 13.2$ Gyr ago, allowing ~0.5 Gyr between the Big Bang and the first stars. We evolve this model for 10 Gyr (i.e. the exact ages of the youngest stars in the mock sample are $\tau = 3.2$ Gyr).

1.3 The Fitting Method

- Introduce a new algorithm that fits the track itself to the [Fe/H] and [α/Fe] abundances of individual stars as opposed to binning the data and fitting the distribution. Though we use chemical abundances as our chief observational quantity, this procedure is highly generic and should in principle be applicable in any region of parameter space where there is intrinsic variation in the density of data points (e.g. isochrones in stellar evolution).
- We make use of `emcee` Foreman-Mackey et al. (2013) to run Markov Chain Monte Carlo (MCMC) fits of parameters in one-zone models of chemical evolution. At each step in parameter space, `emcee` makes a call to the `Versatile Integrator for Chemical Evolution` (`VICE`; Johnson & Weinberg 2020; Griffith et al. 2021; Johnson et al. 2021) to compute the predicted abundances for that selection of parameters. We then compute the likelihood function $L(d|m)$ according to the following procedure.
- For a given realization of a one-zone model with known parameters m and one-zone model predictions μ = ([Fe/H], [α/Fe], log (age)), the likelihood of the data given the model is equal to the product of the likelihoods of each individual data point:

$$L(d|m) = \prod_i L(d_i|m) \tag{7a}$$

$$\implies \ln L(d|m) = \sum_i \ln L(d_i|m). \tag{7b}$$

However, for a given model m, there is no guaranteed way of knowing which point m_j along the computed [α/Fe]-[Fe/H] track should correspond to some data point d_i. We therefore marginalize over the

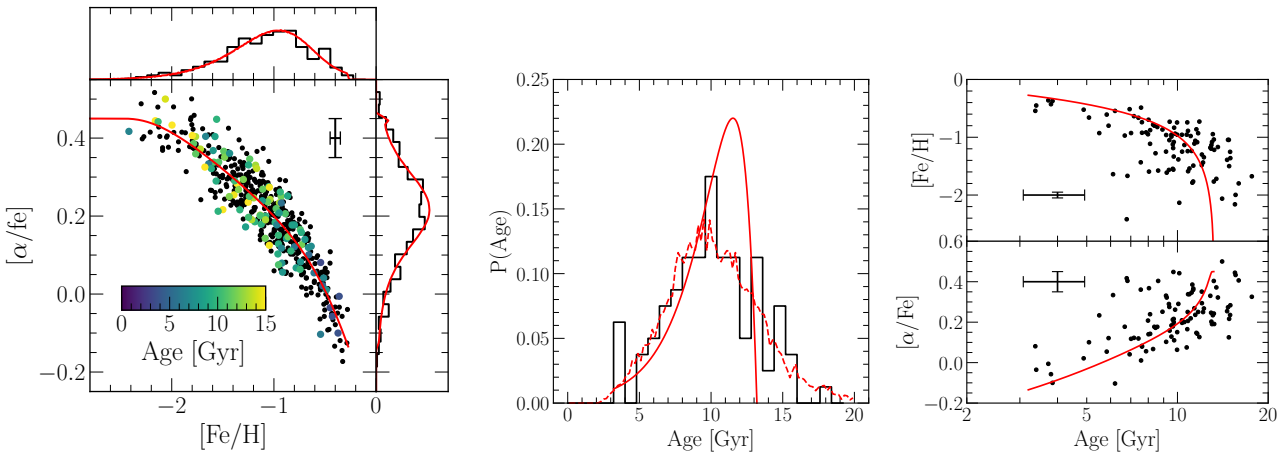

Figure 1. Left: Our fiducial mock sample in the [α/Fe]-[Fe/H] plane. There are $N = 500$ stars with abundance uncertainties of $\sigma([\text{Fe/H}]) = \sigma([\alpha/\text{Fe}]) = 0.05$ as indicated by the errorbar. $N = 100$ of the stars have age information available with an artificial uncertainty of $\sigma(\log_{10}(\text{age})) = 0.1$ as indicated by the colorbar. The red line denotes the evolutionary track in the gas-phase from the one-zone model that generated the mock. On the top and right, we show the marginalized distributions in [α/Fe] and [Fe/H], with red lines denoting the known distribution. **Center**: The mock (black, binned) and known (red) age distributions. The dashed red line indicates the age distribution that is obtained by sampling $N = 10^4$ rather than $N = 500$ stars and assuming the same age uncertainty of $\sigma(\log_{10}(\text{age})) = 0.1$. **Right**: The age-[Fe/H] (top) and age-[α/Fe] (bottom) relation for the mock sample, with artificial uncertainties denoted by the error bars on each panel. The red lines denotes the known relations for the gas-phase.

entire track for every data point d_i by summing the likelihoods from all m_j model vectors:

$$L(d_i|m) = \sum_j L(d_i|m_j) \tag{8a}$$

$$\implies \ln L(d|m) = \sum_i \ln\left(\sum_j L(d_i|m_j)\right) \tag{8b}$$

- We relate the data point d_i and the model point m_j with the relation $L(d_i|m_j) \propto e^{-\chi^2/2}$ with $\chi^2 = \Delta_{ij} C_i^{-1} \Delta_{ij}^T$, where $\Delta_{ij} = \mu_{i,\text{data}} - \mu_{j,\text{model}}$ (i.e. the difference between a pair of data and model vectors) and C_i^{-1} is the inverse covariance matrix of the ith data point.
- Chemical evolution tracks, however, have real, intrinsic variations in the density of points along the track. In one case, a high density of data points may simply reflect the fact that the model vector $\mu_{j,\text{data}}$ is not far from the vector from the previous timestep $\mu_{j-1,\text{data}}$. In another case, a high density of data points may reflect the fact that the star formation rate was high when the galaxy was passing through some region of parameter space. The density of points in the data may also vary because of non-uniform sampling.

REFERENCES

Andrews B. H., Weinberg D. H., Schönrich R., Johnson J. A., 2017, ApJ, 835, 224
Chabrier G., 2003, PASP, 115, 763
de los Reyes M. A. C., Kirby E. N., Ji A. P., Nuñez E. H., 2022, ApJ, 925, 66
Foreman-Mackey D., Hogg D. W., Lang D., Goodman J., 2013, PASP, 125, 306
Griffith E. J., Sukhbold T., Weinberg D. H., Johnson J. A., Johnson J. W., Vincenzo F., 2021, ApJ, 921, 73
Hurley J. R., Pols O. R., Tout C. A., 2000, MNRAS, 315, 543
Johnson J. W., Weinberg D. H., 2020, MNRAS, 498, 1364
Johnson J. W., et al., 2021, MNRAS, 508, 4484
Kalirai J. S., Hansen B. M. S., Kelson D. D., Reitzel D. B., Rich R. M., Richer H. B., 2008, ApJ, 676, 594
Kobayashi C., Karakas A. I., Lugaro M., 2020, ApJ, 900, 179
Kroupa P., 2001, MNRAS, 322, 231
Larson R. B., 1974, MNRAS, 166, 585
Leroy A. K., Walter F., Brinks E., Bigiel F., de Blok W. J. G., Madore B., Thornley M. D., 2008, AJ, 136, 2782
Maeder A., Meynet G., 1989, A&A, 210, 155
Miller G. E., Scalo J. M., 1979, ApJS, 41, 513
Salpeter E. E., 1955, ApJ, 121, 161
Spitoni E., Silva Aguirre V., Matteucci F., Calura F., Grisoni V., 2019, A&A, 623, A60
Spitoni E., et al., 2021, A&A, 647, A73
Tacconi L. J., et al., 2018, ApJ, 853, 179
Weinberg D. H., Andrews B. H., Freudenburg J., 2017, ApJ, 837, 183